Hindawi
International Journal of Energy Research
Volume 2023, Article ID 2282746, 14 pages
https://doi.org/10.1155/2023/2282746

Research Article

Microporous MOF-5@AC and Cu-BDC@AC Composite Materials for Methane Storage in ANG Technology

Niloufar Yadavar Nikravesh, Mojtaba Beygzadeh, and Mehrdad Adl

Department of Energy, Materials and Energy Research Center, P.O. Box: 14155-4777, Tehran, Iran

Correspondence should be addressed to Mojtaba Beygzadeh; m.beygzadeh@merc.ac.ir

Received 25 September 2022; Revised 13 November 2022; Accepted 18 November 2022; Published 3 February 2023

Academic Editor: Semen Klyamkin

Novel composites (MOF-5 and Cu-BDC) based on economically activated carbon have been developed to investigate methane adsorption capacity for ANG applications. The composites were synthesized by adding MOFs precursor in two different weight percent (10% and 40%) to commercial activated carbon under solvothermal conditions (110-120°C). The synthesized adsorbents were characterized by FT-IR, XRD, SEM, EDS, and BET techniques to gather information about their crystallinity, morphology, and specific surface area. A methane uptake measurement system based on the volumetric method was made to obtain methane adsorption capacity on each composite. Then, the amount of methane adsorption for each one was calculated, and the experimental data were compared with different isotherm adsorption models appropriate for gas adsorption, including Langmuir, Freundlich, and Dubinin-Radushkevich. This comparison showed that the best fitting belonged to the Langmuir isotherm model. Also, stability and kinetic studies were done for two MOF-$5_{40\%}$ @AC and Cu-$BDC_{40\%}$ @AC composites. In the kinetics study, experimental data were compared and analyzed in terms of pseudo-first order, pseudo-second order, and intraparticle diffusion models. The kinetics study showed that methane adsorption happens very fast on the synthesized adsorbents. The amount of methane adsorption at 35 bar and room temperature for pure activated carbon was specified as 4.32 mmol/g. The 10% and 40% of Cu-BDC with activated carbon are 5.59 mmol/g and 6.85 mmol/g, respectively. The capacity of MOF-$5_{10\%}$ @AC and MOF-$5_{40\%}$ @AC composites were obtained at 5.9 mmol/g and 7.3 mmol/g, respectively. Increasing methane uptake (70%) was obtained by adding 40 wt.% of MOF-5 to commercial activated carbon.

1. Introduction

A worldwide increase in gaseous fuels has increased the energy demand-supply for industries today. During the following decades, natural gas demand is expected to rise, as estimates predict it will reach over 5000 billion cubic meters by 2040 [1]. Furthermore, increasing the level of CO_2 in the atmosphere, mainly from fossil fuels, contributes to global warming and acts as an unwelcome molecule. Although natural gas (NG) is a fossil fuel source of global warming, it still has some advantages compared to petroleum and coal. Due to the highest hydrogen-to-carbon ratio (octane number = 107.5), the combustion of methane, which is the major constituent of natural gas, produces the smallest amount of CO_2 for each unit of released heat [2]. There are three essential methods for the storage of natural gas that differ from each other on a gas-state basis: CNG (Compressed Natural Gas), LNG (Liquefied Natural Gas), and ANG (Adsorbed Natural Gas). In the ANG method, natural gas is stored on porous materials at ambient temperature and relatively lower pressure (<40 bar) [3]. The quantity of adsorption capacity is different for each adsorbent. The Department of Energy (DOE) has issued >0.5 $g_{CH4}/g_{sorbent}$ as an appropriate natural gas adsorption capacity at a reasonable pressure and temperature range (298 K and 35 bar) for a promising adsorbent. [4]. Generating an adsorbent with high gas adsorption capacity and low cost of production is one of the main challenges facing the development of the ANG method [3].

The adsorption process can be used as a promising technology for both gas capture and storage. So far, several types of porous adsorbents have been developed, such as zeolites,

metal-organic frameworks, porous polymers, porous silica, and porous carbons [3, 5]. Among the porous materials, activated carbon and zeolites have been the most studied microporous materials used as a sorbent to store gases such as methane [4] and hydrogen [6]. Several studies have been performed on the usage of activated carbon for methane adsorption, such as Brazilian coconut shells modified by H_3PO_4 [7], activated carbons from coal/zinc chloride [8], and rice husk (AC-RH). [9]. The performance of prepared activated carbon was compared with the commercial sample (SRD-21) [10]. The cost of adsorbents in the development of a cost-effective methane storage system is one of the major challenges in large-scale ANG storage; so, increasing the capacity of inexpensive commercial carbon adsorbents with new advanced materials such as MOFs can be a new way to commercialize [3].

In recent years, metal-organic frameworks (MOFs) have been considered an advanced porous material in gas adsorption. MOFs have a very high specific surface area, tunable pore size, and large accessible pore volume. MOFs are assembled by the coordination chemistry of metal ions or their clusters and organic linkers and are a useful porous crystalline material in many industries [11]. Compared with other porous materials such as activated carbon, silica, and zeolites, MOFs have better potential as adsorbents, including tunable pores, rich active sites, and selectable functional groups [12]. The first measurement of methane uptake by porous MOFs can be dated to 1977 by Kondo et al. [13]. Kondo et al. [13] used the weighted method to measure the adsorption rate. The adsorption rate was reported at 30 bar, and the ambient temperature of 52 cm^3/g [14]. Subsequently, in 2002, Eddaoudi et al. examined the methane uptake capacity of the isoreticular MOFs material. The methane adsorption capacity was reported for IR-MOF-6 and IR-MOF-1 at a temperature of 298 K and pressure of 35 bar 155 cm^3/cm^3 (STP) and 135 cm^3/cm^3 (STP), respectively [15]. In addition, methane storage capability in HKUST-1 has been studied by several researchers, and its adsorption capacity was reported as 3160 cm^3/cm^3(STP) [16]. Yet, MOFs have some characteristics known as obstacles to using their full potential. A large number of MOFs have been reported for methane storage. Their methane adsorption capacities are often higher than the best-activated carbons. MOF-5 and Cu-BDC are well-studied MOFs containing metal ions (copper and zinc) as the inorganic component and terephthalate ligands (BDC) as the inexpensive petrochemical organic binder coordinated based on 2D layers connected by hydrogen bonds within the bulk crystal. IRMOF-1 (MOF-5) has Zn_4O clusters (the primary adsorption site) and a ZnO_2 site, which makes it a promising adsorbent for methane adsorption at low temperatures [17]. Also, studies on methane adsorption with high capacity at ambient temperature for Cu-BDC MOF have been reported [18].

Most MOFs are nonelectricity conductive and not sturdy against water/vapor, high temperature, and robust electron beams. They were found in powder with weak mechanical strength, and the configurations are not optimal for subsequent processibility [19–21]. The low density of atoms in MOFs results in a high diffusion coefficient and affects the final capacity of adsorption [11, 22, 23]. There are some ways to manage the challenges mentioned. One of them is building MOF-based composites [24, 25]. Among them, MOF-carbon composites (a combination of metal-organic frameworks and carbon-based materials) have received much attention due to their unique, extraordinary characteristics such as high mechanical and elastic strength, chemical and thermal robustness, low weight, low toxicity, and sometimes low cost improves MOFs weaknesses [25–27]. Many studies have investigated MOF-carbon composites. In recent years, most of the studies in this field have focused on MOF-Go (graphite or graphene oxide) composite [24, 28, 29]. Generally, in most of the previous studies about the composite of MOFs and activated carbon materials, the base of the composite was constituted MOF, and activated carbon was added to the composite as the secondary material [12]. Furthermore, the thermal stability, mechanical strength, and resistance to the humidity of the MOFs were improved by compositing them with carbon-based materials as a protective shield [12].

The present work investigated the incorporation of microporous Cu-BDC and MOF-5 framework into commercial activated carbon and their effect on the volumetric methane storage capacity. We prepared MOF-5@AC and Cu-BDC@AC by varying the amount of MOF from 10 to 40 wt.% through a one-pot and straightforward solvothermal method. Then, the methane uptake was measured on the synthesized adsorbents by a volumetric method at 298 K and up to 35 bar. Moreover, the SRK equation of state was used to obtain the amount of adsorption, and isotherm curves were plotted and fitted.

2. Experiment

2.1. Materials. $Zn(NO_3)_2.4H_2O$, $Cu(NO_3)_2.3H_2O$, terephthalic acid, N,N-dimethylformamide (DMF), and dichloromethane were purchased from Merck Co. Commercial activated carbon (815 $m^2 g^{-1}$) was obtained from Caware Int'l Corp (Taiwan). Autoclaving reagent bottle 100 ml, 250 ml with GL45 thread blue cap was prepared from Simax®.

2.2. Synthesis of MOF-5 and MOF-5@AC Composite. MOF-5 was synthesized by the previously reported procedures [30]. For a typical synthesis, $Zn(NO_3)_2.4H_2O$ (1.45 g, 6 mmol) and terephthalic acid (0.33 g, 2 mmol) were mixed in 80 ml DMF. The resulting mixture was stirred for 20 minutes and then transferred to a glass reagent bottle heated for 7 h at 100°C under solvothermal conditions. Then, the white precipitate obtained was washed with the predried DMF three times and immersed in CH_2Cl_2. The solvent was exchanged daily for 24 h, exchanged once every 8 h, and was finally dried at 60°C under a high vacuum for 12 h. Similarly, MOF-5@AC composite was synthesized by adding activated carbon to the terephthalic acid solution. The MOF-5@AC composites with different MOF-5 ratios (10 and 40%) were synthesized by adjusting the amount of

activated carbon, and they are referred to as MOF-$5_{10\%}$ @AC/and MOF-$5_{40\%}$ @AC in the rest of this paper.

2.3. Synthesis of Cu-BDC and Cu-BDC@AC Composite. Cu-BDC was synthesized as previously reported [31]. In a typical preparation, a mixture of $Cu(NO_3)_2.3H_2O$ (1.45 g, 6 mmol), terephthalic acid (1 g, 6 mmol), and DMF (75 ml) were stirred for about 20 min to get a clear solution, then transferred to a glass reagent bottle heated at 110°C for 36 h. The blue precipitate was obtained and washed with DMF several times, and it was dried in an oven at 220°C for 24 h. The Cu-BDC@AC composite was prepared by adding activated carbon to well-dissolved MOF precursors in the same procedure described for Cu-BDC. The obtained sample was washed with DMF several times at 24 h and finally dried in an oven at 220°C for 24 h. Samples with Cu-BDC weight ratios of 10%, and 40% were synthesized by changing the amount of activated carbon, and the samples are referred to as Cu-$BDC_{10\%}$ @AC and Cu-$BDC_{40\%}$ @AC after here.

2.4. Characterization. Fourier-transform infrared (FT-IR) spectra were obtained at room temperature on a Brucker V33 instrument for the chemical structure and binding properties of activated carbon MOF and composite. X-ray powder diffraction patterns were carried out by an X'pert MPD Philips DW371 with Cu Kα radiation ($\lambda = 1.5406$ Å). The morphology of prepared samples was also observed by scanning electron microscopy (SEM, TESCAN VEGA-XMU). Surface area and pore size analyses were made from an analyzer (Belsorp-Mini II, Gemini 2375 (Bel Japan Inc.)) using nitrogen adsorption measurements at liquid nitrogen temperature (77 K). Firstly, each sample was degassed under the vacuum (10-5 Torr) at 150°C for 6 h to remove any entrapped guest molecules.

2.5. Design of Experimental. In order to obtain the adsorption capacity of methane on different synthesized adsorbents, the static volumetric method was used. For this purpose, a volumetric-based apparatus was made. As is shown in Figure 1, this apparatus consists of a reference cell with a specified volume and a sample cell used to measure the methane uptake. The apparatus was placed in a constant-temperature water bath for the isothermal system could maintain a constant temperature. In the inlet line, two main valves were considered for the injection of methane gas for measuring the adsorption and helium gas as the inert gas for determining the amount of dead volume. This apparatus was equipped with a vacuum pump and a heater to discharge residual gas in the whole apparatus. A line that was directed to the atmosphere was considered for gas venting. The operating condition for this apparatus is 35 bar at ambient temperature. A pressure transducer was mounted between two cells to measure the pressure of the reference cell before and after gas injection to the adsorption cell.

2.6. Adsorbent Test in Operating Conditions. After preparing the measuring apparatus, the following procedure was used to collect the experimental adsorption capacity for synthesized adsorbents.

At first, a weighted adsorbent was introduced into the adsorption cell. Before beginning the measurements, the adsorbents were degassed at about 150°C under vacuum pressure for about 4 hours. The adsorption cell was cooled down to the ambient temperature to measure the amount of gas adsorbed. Later, the pressure regulator on the methane cylinder was fixed on 5 bar, gas was injected into the reference cell, and the inlet valve was closed. The valve between the two cells was opened in the next step, and the pressure drop after receiving to equilibrium condition was recorded. The condition of equilibrium was the condition at which the pressure in the sample cell stabilized. This observation confirmed that methane adsorption could occur when the adsorbent and methane came into contact. The mentioned step was repeated for different pressures up to 35 bar to achieve the isotherm. The pressure drops, which were observed in these steps, refer to adsorption and pressure drop caused by void volume and pipelines. Therefore, to determine the void volume of the adsorbents, a known amount of helium (as an inert gas that cannot be adsorbed by adsorbent) was injected in the next step, and a pressure drop was recorded.

The void volume of the cell at equilibrium was determined from measured values of temperature, pressure, and amount of helium injected into the cell by using the following equation:

$$V_2 = \frac{P_{1_{He}}/Z_{1_{He}}}{P_{2_{He}}/Z_{2_{He}}} V_1, \tag{1}$$

where V_2 represents the volume of the sample cell and other valves and connections after helium introducing to the sample cell and V_1 represents the volume before opening the valve between two cells. Also, P_{1He}, Z_{1He}, and P_{2He}, Z_{2He} shows the pressure and compressibility factor of helium in the reference cell before and after the equilibrium, respectively.

$$V_{void} = V_2 - V_1. \tag{2}$$

The helium void volume (V_{void}) includes all the volumes of the cell section, exclusive of the adsorbent volume that is impenetrable to helium. Thus, the amount of mole of gases before the equilibrium state was obtained from the sum of gas molecules in the reference cell, the connections and gas molecules in the sample cell are as follows:

The mole of gas in the reference cell

$$n_1 = \frac{P_1 V_1}{Z_1 RT}, \tag{3}$$

where P_1 represents the pressure, V_1 represents the volume, Z_1 shows the compressibility factor of gas injection to the reference cell, and R and T show gas constant and temperature, respectively.

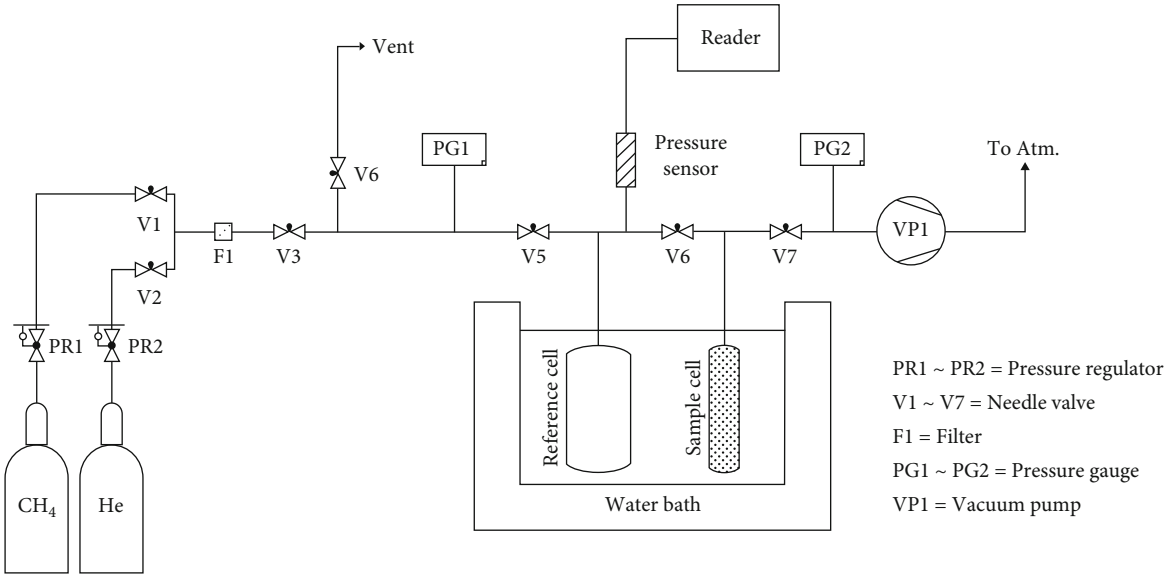

Figure 1: Schematic diagram of the experimental setup.

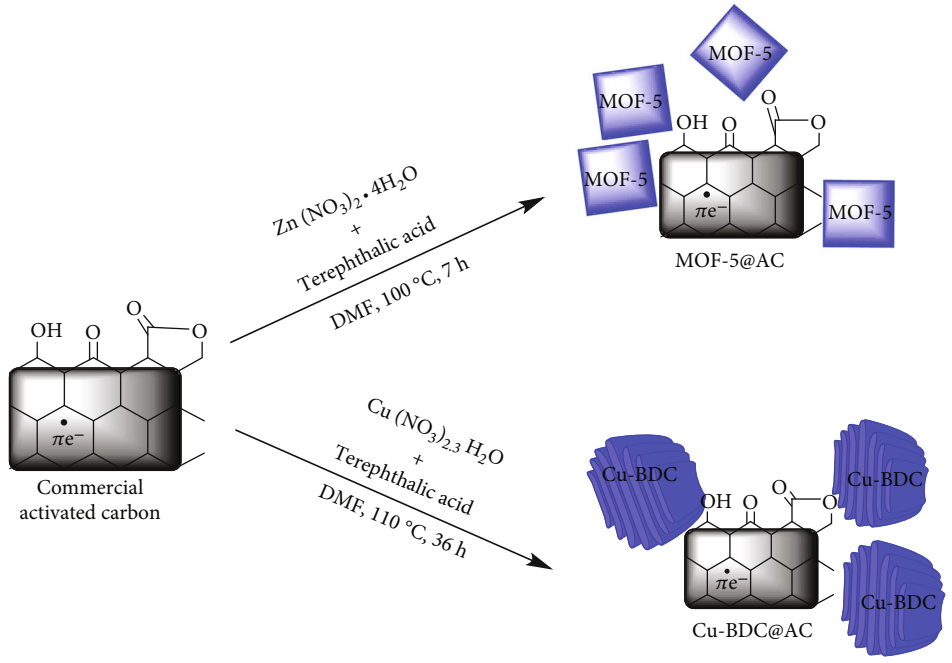

Figure 2: Schematic diagram of synthesizing MOF-5@AC and Cu-BDC@AC composite.

The mole of gas in voids of sample cell

$$n_1' = \frac{P_1' V_{\text{void}}}{Z_1' \text{RT}}, \tag{4}$$

where P'_1 and Z'_1 represent the equilibrium pressure and compressibility factor from previous gas injection stage.

Therefore, the mole of gas before gas injection to the sample cell equals the sum of n_1 and n'_1.

$$n_{\text{total}} = n_1 + n_1'. \tag{5}$$

After opening the valve between the sample and the reference cell, the gases from the reference cell were in contact with the adsorbent. After the equilibrium state, the mole of gas was obtained from the following equation:

$$n_2 = \frac{P_2 V_2}{Z_2 \text{RT}}. \tag{6}$$

It should be mentioned that in all the equations, Z_1 and Z_2 represent the compressibility factor of methane in the reference cell before and after equilibrium, respectively, and P_2 shows the pressure of methane in the reference cell after

equilibrium. Moreover, to determine Z-factor, the SRK equation was used as follows:

$$Z^3 - Z^2 + \left(A - B - B^2\right).Z - A.B = 0, \tag{7}$$

where

$$\begin{aligned} A &= \frac{a.P}{R^2.T^2}, \\ B &= \frac{b.P}{R.T}, \\ a &= a_c.\alpha, \\ a_c &= 0.42747\left(\frac{R^2.T_c^2}{P_c}\right), \\ \alpha^{1/2} &= 0.48 + 1.574\omega - 0.176\omega^2, \\ b &= 0.08664\left(\frac{R.T_c}{P_c}\right), \end{aligned} \tag{8}$$

where T_c, P_c, and ω are critical temperature, critical pressure, and acentric factor for methane gas.

Therefore, the amount of adsorbed gas in one stage is equal to

$$\Delta n_{\text{adsorbed}} = n_1 + n_1' - n_2. \tag{9}$$

The procedure was repeated to increase the pressure of methane incrementally. Finally, the estimate of the total amount of gas adsorbed, n_{ads} at the i^{th} step was calculated from the following equation:

$$n_{\text{ads}} = \Delta n_{\text{ads1}} + \Delta n_{\text{ads2}+\cdots\cdots+}\Delta n_{\text{adsi}}. \tag{10}$$

Also, to determine the adsorbent's capacity, the amount of gas adsorbed was divided into the weight of the adsorbent as follows:

$$q = \frac{n_{\text{absorbed}}}{W_{\text{absorbent}}}. \tag{11}$$

3. Results and Discussions

The schematic illustration of the formation of MOF-5 and Cu-BDC on the activated carbon resulting in MOF-5@AC and Cu-BDC@AC composites is shown in Figure 2. The reaction conditions are elementary using a facile one-pot solvothermal method.

3.1. Characterization

3.1.1. XRD Patterns. Figures 3(a)–3(d) compare the XRD (X-ray Diffraction) patterns of MOF-5, MOF-5@AC, Cu-BDC, and Cu-BDC@AC. Figure 3(a) represents the XRD pattern of the MOF-5 with high intensity of the characteristic peaks ($2\theta = 6.8^\circ$, 9.6°, 13.6°, and 24.7°), which are consistent with the results reported in the literature, confirming the successful formation of MOF-5. Figure 3(b) shows the formation of MOf-5 in the composite based on activated carbon, which

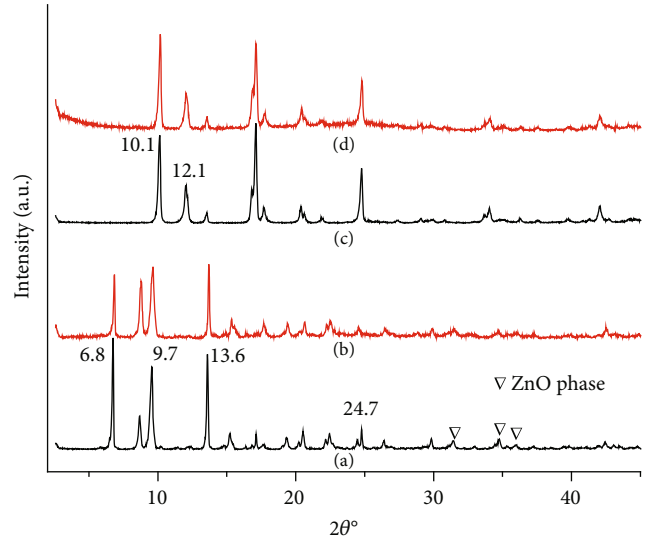

Figure 3: Powder X-ray diffraction patterns of (a) MOF-5, (b) MOF-5@AC composite, (c) Cu-BDC, and (d) Cu-BDC@AC composite.

confirms the successful formation of the MOF-5@AC composite because the amorphous carbon does not have a specific crystallinity. Furthermore, a small amount of zinc species impurity is also visible in the phase that was probably entrapped in the framework MOF-5 [30, 32]. Figure 3(c) represents the characteristic peaks of Cu-BDC, which appeared at $2\theta = 10.1^\circ$ and 12.1°, representing (001) and (020) planes of crystal structure, respectively, are matched well with XRD patterns, which have been reported before with no impurity. Consequently, The XRD patterns of Cu-BDC@AC (Figure 3(d)) composites show the same diffraction patterns as Cu-BDC, confirming that the incorporation of activated carbon to Cu-BDC MOFs follows those reported in the literature [33, 34].

3.1.2. SEM and EDS. The texture of the as-synthesized of MOF-5, MOF-5@AC, Cu-BDC, and Cu-BDC@AC composite can be observed in scanning electron microscopy (SEM) images presented in Figure 4, respectively. The SEM image (Figure 4(a)) shows that the MOF-5 particles are uniform with a regular cubic with an average size of about 30-40 μm [32]. Figure 4(c) shows that the Cu-BDC MOF particles are uniform with well-formed cubic microcrystals, and their average edge length is about 9.3 μm. Their morphology is compatible with the previous results that were achieved from hydrothermal synthesis [35]. Comparing the SEM images of MOF-5@AC and Cu-BDC@AC composite (Figures 4(b) and 4(d)) with primary MOFs exhibit the successful formation of MOf-5 and Cu-BDC based on activated carbon. Furthermore, the EDS (Energy Dispersive Spectroscopy) spectra in Figures 4(e) and 4(f) show that MOF-5 and Cu-BDC have been successfully introduced in activated carbon composites resulting in zinc and copper element presence in EDS analysis.

3.1.3. FT-IR Results. FT-IR spectra, as shown in Figure 5, are obtained to gain more detailed information about the

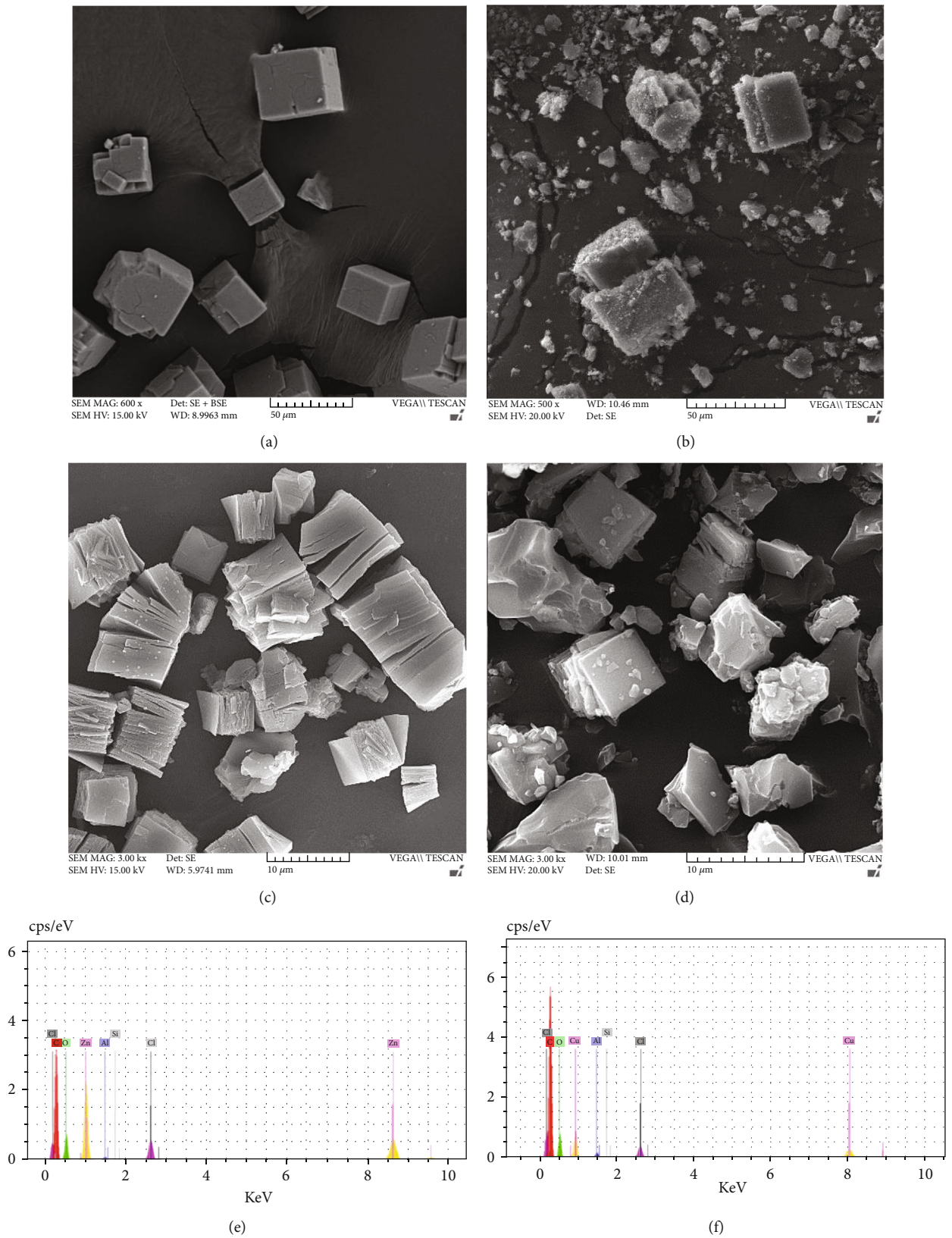

Figure 4: SEM images of (a) MOF-5, (b) MOF-5@AC composite, (c) Cu-BDC, and (d) Cu-BDC@AC composite and EDS spectra of (e) MOF-5@AC and (f) Cu-BDC@AC composite.

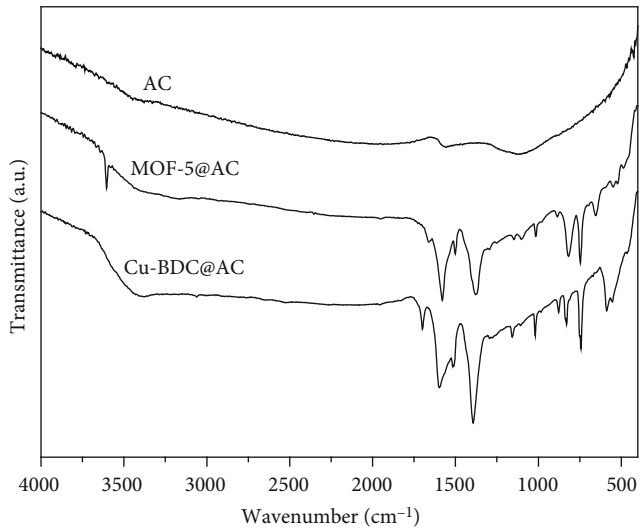

Figure 5: FT-IR spectra of activated carbon, MOF-5@AC, and Cu-BDC@AC composite.

structure of the synthesized composites. The IR spectrum of the original activated carbon shows no significant bands, but after the formation of the composite, all peaks of MOF absorption spectra appear. In the FT-IR spectrum of MOF-5@AC, two absorption bands, 2948.2 and 2870.7 cm^{-1}, are assigned to C-H stretching vibrations of the methylene group of remaining DMF in the composition of synthesized MOF. The vibration bands appearing in 1700–1400 cm^{-1} are assigned to the carboxylic functionality of the 1,4-benzenedicarboxylate. The strong peak appearing at 1758.1 cm^{-1} can be attributed to the C=O stretching vibration of the carboxylate group of MOF-5. All dedicated absorption peaks of Cu-BDC are observed in the infrared spectrum of the Cu-BDC@AC composite. The sharp absorption peaks at 1602 and 1398 cm^{-1} belong to the carboxylate groups' asymmetric and symmetric stretching modes, respectively. The bands at 1512 and 743 cm^{-1} are assigned to the vibrations of the phenyl ring. The vibration bands at 468 and 556 cm^{-1} can be assigned to the Cu–O stretching vibration [30, 36]. All these points illustrate that MOF-5 and Cu (BDC) had developed. SEM results also support this assumption.

3.1.4. N_2 Adsorption–Desorption Isotherms Analysis. Figure 6 shows the N_2 adsorption-desorption isotherms at 77 K and pore size distributions obtained by the MP-plot method for various samples with the structural parameters listed in Table 1. According to the IUPAC classification, the isotherms obtained for all samples are of type I, which is typical for microporous materials. The isotherm of AC and MOF-5 belongs to type I in the IUPAC classification, which is a characteristic of microporous materials. Cu-BDC revealed the isotherm type I with H_2 hysteresis, which is related to microporous material. The hysteresis loop observed at high relative pressure implies the existence of some mesopores. The pore size distributions from the MP method of as-synthesized MOFs and composites are shown in Figures 6(c) and 6(d), which are about 0.6 nm specific to microporous materials.

3.2. Test of Adsorbents. This section examines and discusses methane uptake on the synthesized adsorbents. Figure 7 demonstrates the CH_4 uptake capacities as a function of pressure for pure adsorbents. Also, the amount of methane uptake on the composite of 10 and 40 weight percent of MOF-5 and Cu-BDC based on activated carbon compared with commercial activated carbon has been in Figure 8. The capacity of CH_4 in adsorbents is usually proportional to their surface areas. Despite the higher surface area in the commercial activated carbon, a lower methane uptake has occurred compared with the synthesized MOFs. MOFs have higher CH_4 uptake than conventional porous materials such as carbon and zeolites. The mechanism of the enhanced uptake is due to the existing three sites: the center of the cluster, pore cages of the phenyl rings, and unsaturated metal ion active sites located at the center of the cavity. van der Waals contact and partial π-HC interactions can significantly interact between methane and adsorption centers [37–39]. A clear result of increasing the amount of MOF used in the composite is that it significantly increases the CH_4 uptake. By comparing the amount of gas uptake on the different adsorbents, this result is obtained that MOF-5 has the highest capacity of methane uptake than other composites and activated carbon. However, adding MOFs to the composite indicated a positive effect in increasing methane uptake.

Table 2 compares the amount of methane uptake in the synthesized adsorbents in this study with other adsorbents reported in the literature. To have a better comparison, the sorbents are selected from the articles having the same test conditions, including pressure and temperature. This comparison shows that the amount of gas adsorption on a specific adsorbent may be different, and it is due to the different conditions of synthesis and tests that are taken on the adsorbents.

3.3. Adsorption Kinetic Studies. To investigate the correlation of methane adsorption and predict the rate-limiting step in MOF-$5_{40\%}$ @AC and Cu-$BDC_{40\%}$ @AC, the gathered experimental data are fitted to two regular models, pseudo-first-order and pseudo-second-order models. The reason for selecting these models is their simplicity in describing the interaction rate in the solid-gas adsorption process. The equation of the pseudo-first-order model is defined as follows:

$$q_t = q_e\left(1 - e^{k_1 t}\right), \tag{12}$$

where q_e and q_t (mmol/g) represent the amount of methane gas adsorbed at equilibrium and at time t (min). Also, k_1 (1/min) is the constant rate of adsorption.

When pressure increases at a constant temperature, k_1 is increased. It means that at higher pressures, the methane uptake will be decreased. Otherwise, the required time for reaching the equilibrium state will be increased.

Also, pseudo-second-order was another kinetic model which is used in this study with the following equation:

$$q_t = \frac{q_e^2 k_2 t}{1 + q_t k_2 t}, \tag{13}$$

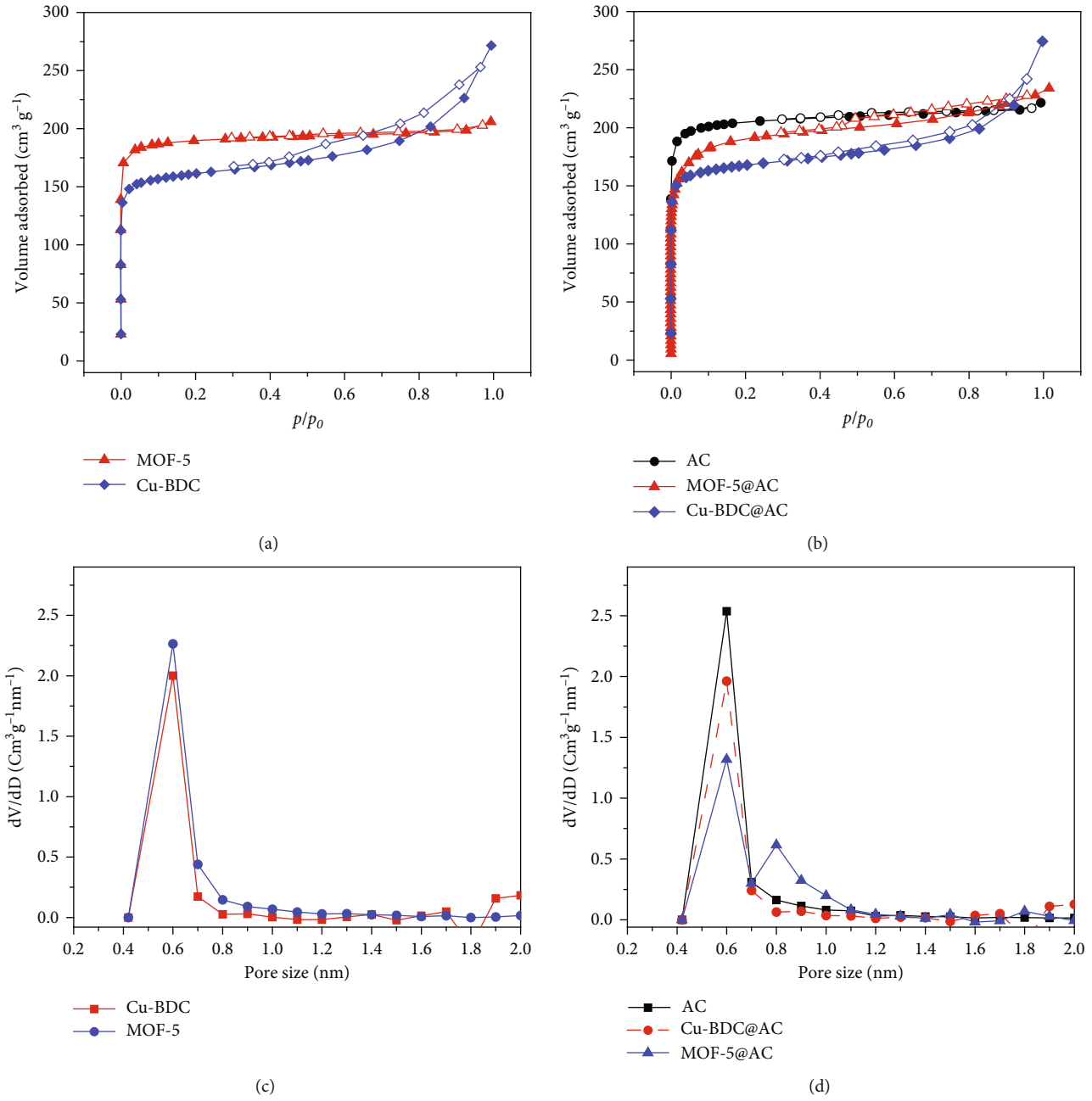

FIGURE 6: N_2 adsorption-desorption isotherms of (a) MOF-5, Cu-BDC, (b) AC, MOF-5@AC, and Cu-BDC@AC, (c) and (d) pore size distribution of MOF-5, Cu-BDC, and composites obtained by MP-plot.

where q_e and q_t (mmol/g) represent the amount of methane gas adsorbed at equilibrium and at time t (min), also, k_2 (g/mmol.min) is the constant rate of the adsorption.

According to the result of the pseudo-second-order model, when pressure increases, k_2 will be increased. It represents a low repulsion in methane molecules, which increases diffusivity [49]. Also, by comparison of R^2 values of pseudo-first-order and second-order in Table 3, it seems that the amount of R^2 values of the pseudo-first-order is relatively higher than the second-order model. The pseudo-first-order model better matches theoretical and experimental data [50]. On the other hand, since pseudo-first-order and pseudo-second-order cannot show the diffusion mechanism, the extracted results from kinetic models have been analyzed by the intraparticle diffusion model [51]. The intraparticle diffusion equation is defined as the following equation:

$$q_t = k_p t^{0.5} + C. \tag{14}$$

In Equation (14), k_p is defined as the intraparticle diffusion rate constant (mmol.g^{-1} min$^{-0.5}$) and t represents time (min).

In Figure 9 the plot of methane adsorption versus $t^{0.5}$ is shown. According to the gathered data, the methane

Table 1: Textural characteristics of samples.

Samples	BET surface area		Mean pore diameter (nm)	Total pore volume ($cm^3\ g^{-1}$)
	BET ($m^2\ g^{-1}$)	Langmuir ($m^2\ g^{-1}$)		
Commercial AC	815	920	1.67	0.342
MOF-5	760	847	1.67	0.317
Cu-BDC	633	740	2.62	0.416
MOF-5@AC	711	866.3	2.00	0.355
Cu-BDC@AC	657.2	766	2.53	0.416

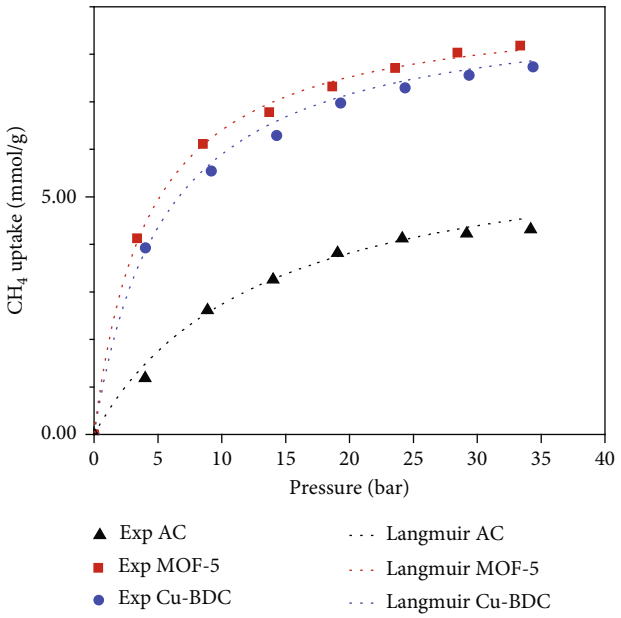

Figure 7: CH_4 uptake of the AC, MOF-5, and Cu-BDC adsorbents (experimental data and Langmuir's model).

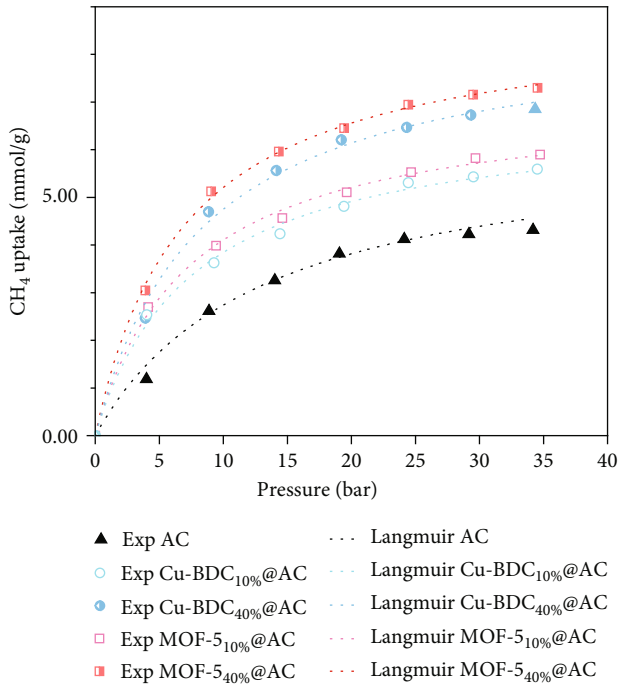

Figure 8: CH_4 uptake of the MOF-$5_{40\%}$ @AC, MOF-$5_{10\%}$ @AC, Cu-$BDC_{40\%}$ @AC, Cu-$BDC_{10\%}$ @AC, and AC adsorbents (experimental data and Langmuir's model).

adsorption process has high-speed kinetics, and the adsorption reaches the equilibrium state in the early minutes. Equation (14) is a linear equation with the intercept C, and the value of zero for the intercept shows that intraparticle diffusion is the only controller of the adsorption process. When the amount of C is not zero, according to Table 3, it means that the adsorption process is based on the pseudo-first-order kinetic model and intraparticle diffusion [51].

3.4. Adsorption Isotherm Studies. The adsorption isotherms can describe the equilibrium performance of adsorbents in an isotherm process. Many factors, including adsorbents, physical properties of adsorbate, and adsorption process condition, affect adsorption isotherm [42].

Also, adsorption isotherm models explain the interaction between adsorbate fluid and synthesized adsorbents. The extracted data from the adsorption experiment are fitted with three isotherm models, Langmuir, Freundlich, and Dubinin-Radushkevich equilibrium isotherm models. The isotherm constants are reported in Table 4. These isotherm models are used to investigate adsorption conditions, including homogeneous/heterogeneous and monolayer/multilayer. Many different isotherm models can be used to investigate the experimental data; however, these models are selected since they are more appropriate for the gas adsorption process than others [52, 53].

The Langmuir adsorption isotherm model is a straightforward and appropriate isotherm model used for homogeneous surfaces of sorbent to explain monolayer and chemical adsorption in the gas-solid phase. This model is the most common isotherm model to investigate methane and carbon dioxide of activated carbon [52, 54]. According to this isotherm model, the surface of a solid adsorbent is a completely uniform and homogeneous surface composed of one type of material, and there is no preferred place for adsorption on its surface. All places have the same priority for adsorption. Also, each site does not adsorb more than one molecule; in such a situation, a single layer of molecules will be adsorbed on the solid surface [55]. The equation of the Langmuir isotherm model is defined as follows:

$$q_e = \frac{bP}{1 + bP} q_m, \tag{15}$$

Table 2: Comparison of the methane adsorption capacity of the synthesized adsorbents with others.

MOFs	Framework density D_c (g/cm^3)	BET surface area (m^2/g)	Total uptake (cm^3/cm^3)	(cm^3/g)	(mmol/g)	Conditions pressure (bar)/temperature (K)	References
MOF-905	0.549	3490	145	264	11.78	35/298	[40]
LIFM-82	0.922	1624	196	214	9.55	35/298	[40]
NU-125	0.589	3286	182	315	14.06	35/298	[40]
AC1	0.5	1060.3	—	—	5.11	35/298	[10]
AC2	0.58	363.3	—	—	3.06	35/298	[10]
AC3	0.39	1177.7	—	—	7.92	35/298	[10]
AC4	0.49	1050.8	—	—	5.18	35/298	[10]
LIFM-83	0.917	1715	192	—	9.36	35/298	[41]
MOF-5	0.59	1870	135	228	10.18	36/298	[14]
IR-MOF1	0.59	—	128.29	217.45	9.71	35/298	[42]
MOF-5	0.61	—	135	221	9.87	35/298	[15]
MOF-5	0.593	—	110	185	8.28	35/298	[43]
CMK-3	0.87	950	—	117.33	5.2	35/298	[44]
Cu-BDC	—	624	—	—	3.8	35/298	[45]
Cu-BDC	—	603	—	—	11.58	35/293	[46]
MIL-53(Cu)/CNT	—	1123			13.72	35/298	[47]
$Mn(HCO_2)_2$/graphite	—	280			4.24	1/298	[48]
MOF-$5_{40\%}$ @AC	—	711	—	—	7.3	35/298	This study
MOF-$5_{10\%}$ @AC	—	—	—	—	5.9	35/298	This study
Cu-$BDC_{40\%}$ @AC	—	657	—	—	6.85	35/298	This study
Cu-$BDC_{10\%}$ @AC	—	—	—	—	5.59	35/298	This study
Pure activated carbon	—	815	—	—	4.32	35/298	This study
MOF-5	—	760	—	—	8.18	35/298	This study
Cu-BDC	—	633	—	—	7.74	35/298	This study

Table 3: Kinetic parameters of methane adsorption on the synthesized adsorbents.

Sample	Pressure (bar)	1st order		2nd order		Intraparticle diffusion	
		k_1 (min^{-1})	R^2	k_2	R^2	k_t	C
Cu-$BDC_{40\%}$ @AC	10	19.34517	0.99982	6.12224	0.9974	0.65735	3.23076
	20	24.64329	0.99982	8.6197	0.99882	1.00831	3.92865
	35	34.99325	0.9997	27.65285	0.9989	1.04148	4.506
MOF-$5_{40\%}$ @AC	10	22.61693	0.99867	10.34506	0.99861	0.74586	3.44628
	20	24.23923	0.99837	13.94849	0.99512	0.93451	4.35472
	35	28.8976	0.99997	17.21931	0.99909	0.99	5.08543

where q_m shows the monolayer uptake capacity (mmol/g), b is the affinity coefficient constant (1/bar), q_e represents the amount of gas uptake on the adsorbent (mmol/g), and P is the adsorbed gas pressure (bar). The isotherm constants are shown in Table 4.

The affinity coefficient constant (b) indicates the extent of interaction between the adsorbate and the surface. Therefore, the highest value in MOF-5 indicates that CH_4 has the strongest affinity toward the MOF-5 surface. Also, for evaluating an adsorbent's adsorption capacity, Langmuir's predicted q_m is valuable. Experimentally, measured CH_4 adsorption isotherms for MOF-5 show good compatibility with the single-site Langmuir's model [56].

Freundlich's adsorption isotherm model is suitable for predicting adsorption on heterogeneous surfaces and explaining nonideal processes and multilayer surfaces [52]. Therefore, it could be a good complementary model addition to the Langmuir isotherm model to better investigate heterogeneous and multilayer sites. The main difference between the Langmuir and Freundlich models is that the Freundlich model is applicable for multilayer adsorption [57]. Freundlich's equation has been shown in the following equation:

$$q_e = k_f P^{1/n}, \tag{16}$$

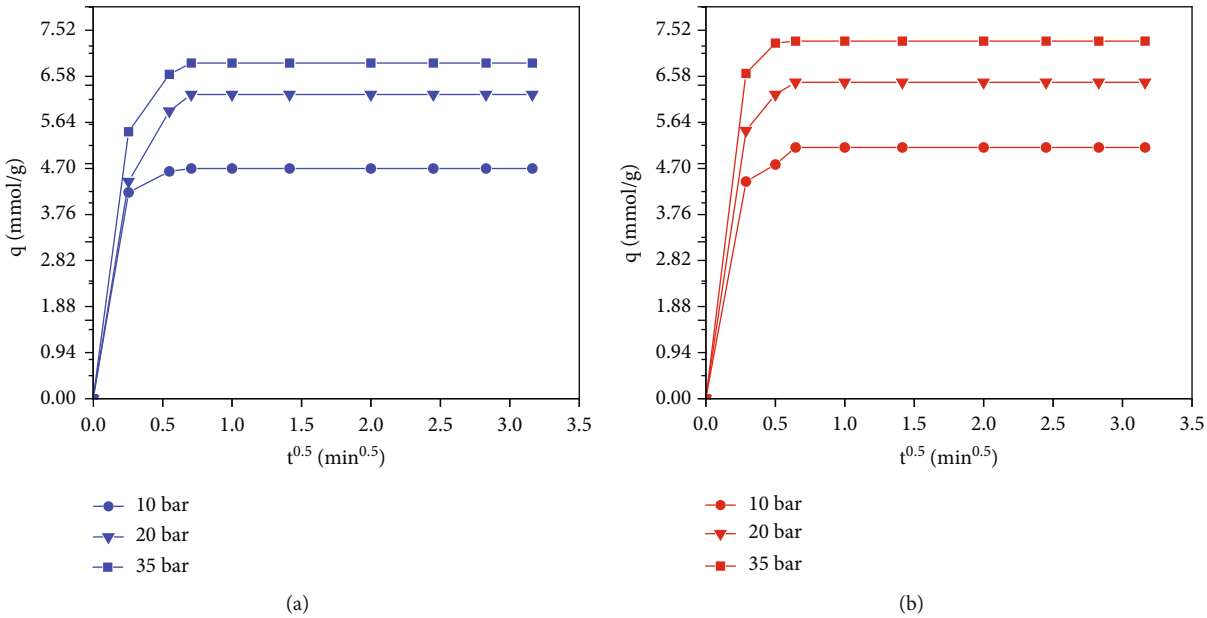

Figure 9: Methane adsorption onto (a) Cu-BDC$_{40\%}$ @AC and (b) MOF-5$_{40\%}$ @AC vs. $t^{0.5}$.

Table 4: Isotherm adsorption parameters of methane on the synthesized adsorbents.

Isotherm model	Parameters	Adsorbent						
		MOF-5	Cu-BDC	MOF-5$_{40\%}$ @AC	MOF-5$_{10\%}$ @AC	Cu-BDC$_{40\%}$ @AC	Cu-BDC$_{10\%}$ @AC	AC
Langmuir	b	0.23648	0.18285	0.14266	0.13577	0.12086	0.12988	0.07714
	q_m	9.11192	9.11705	8.85747	7.12896	8.68267	6.80366	6.29136
	R^2	0.99864	0.99886	0.99901	0.9976	0.99529	0.99561	0.99178
Freundlich	k_f	3.24357	2.80105	2.25553	1.76679	1.90782	1.61748	0.89296
	n	3.67202	3.37541	2.898971	2.857551	2.643894	2.779476	2.117881
	R^2	0.97146	0.97647	0.93882	0.98095	0.92319	0.98563	0.92945
Dubinin-Radushkevich	q_m	8.38582	7.95513	7.65061	6.0871	7.30938	5.75872	4.71858
	k	0.01351	0.01565	0.01869	0.01887	0.02092	0.01926	0.02697
	R^2	0.99367	0.99471	0.98483	0.99479	0.96912	0.99521	0.96889

where k_f is the Freundlich isotherm constant (mmol/g) and n is the adsorption intensity and is a heterogeneity factor.

Dubinin-Radushkevich's (D-R) adsorption isotherm model is a semiempirical equation for multilayer surfaces. Initially, the application of this model was for subcritical vapors on micropore materials. Now, it is used to determine chemical and physical gas adsorption in microporous materials [52]. The equation of the D-R model is as follows:

$$q_e = q_m \exp\left(-k\varepsilon^2\right), \longrightarrow \varepsilon = \mathrm{RT} \ln\left(\frac{P_s}{P}\right). \tag{17}$$

In the equation, P_s and P are the saturation vapor pressure and the adsorbate equilibrium pressure, respectively. Also, k value represents the activity coefficient (mol^2/kJ^2), R is the gas constant, and q_m is the maximum amount of adsorption that occurs in monolayer adsorption (mmol/g).

The correlation coefficients (R^2) values of all isotherm models represent which equation is more appropriate for the synthesized adsorbents. The higher R^2 value, the more well-suited an isotherm model is to describe the methane uptake process. By comparing this value in different models, the Langmuir isotherm is the best isotherm model to explain the CH_4 uptake process. Besides, since methane is a nonpolar gas, it tends to be adsorbed on homogeneous surfaces. The Langmuir isotherm model's application for homogeneous materials and R^2 values confirm the homogeneity of the synthesized adsorbents.

3.5. Regenerability of the Adsorbents. Two adsorbents MOF-5$_{40\%}$ @AC and Cu-BDC$_{40\%}$ @AC are selected for further investigation of the reusability and stability. Figure 10(a)

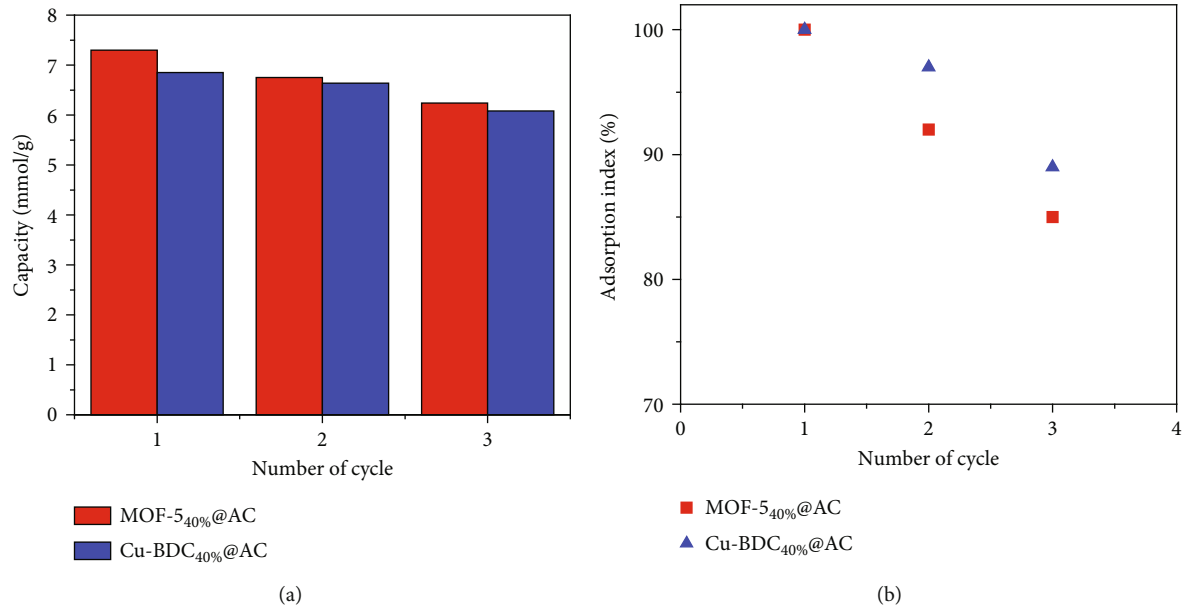

Figure 10: (a) Adsorption capacity of three cycles of MOF-5$_{40\%}$ @AC and Cu-BDC$_{40\%}$ @AC (b) Adsorption index performance of MOF-5$_{40\%}$ @AC and Cu-BDC$_{40\%}$ @AC.

shows that the adsorption capacity of the adsorbents was compared in three cycles, and Figure 10(b) is shown the adsorption index of each adsorbent in each cycle in comparison with the highest capacity of each adsorption. By repeating the test three times and according to the adsorption index, Cu-BDC$_{40\%}$ @AC showed better regenerability than MOF-5$_{40\%}$ @AC. The capacity of Cu-BDC$_{40\%}$ @AC in the second cycle reduced to 0.97 percent of the first cycle, although MOF-5$_{40\%}$ @AC reached 0.92 percent of the maximum capacity. Also, in the last cycle, the capacity of MOF-5$_{40\%}$ @AC is reduced to 0.85 percent of the first cycle, and Cu-BDC$_{40\%}$ @AC was reduced to 0.89 percent.

4. Conclusions

MOF-5@AC and Cu-BDC@AC composites were prepared based on the commercial activated carbon. Since MOFs are not cost-effective, composites of MOFs based on commercial activated carbon could be effective strategies to reduce the cost of the ANG method. The result of experiments on different adsorbents was shown that among activated carbon and composites, MOF-5$_{40\%}$ @AC has the highest amount of methane uptake, equal to 7.3 mmol/g at 35 bar pressure and 298 K temperature. The capacity of MOF-5 was about 90% higher than the pure activated carbon, and by adding 40% MOF-5 to the composite, the methane uptake was increased 70%. Also, more studies, including regenerability and kinetic studies, were done on the composites (MOF-5$_{40\%}$ @AC and Cu-BDC$_{40\%}$ @AC). These studies showed that the recovered adsorbents retain their original porous structure, and Cu-BDC$_{40\%}$ @AC had better stability than MOF-5$_{40\%}$ @AC. Moreover, based on the kinetic studies of these two adsorbents in three different pressures, it was indicated that sorption kinetics happens very fast and is suitable for practical applications of methane adsorption. The good adjustment of experimental data with pseudo-first-order indicated that physisorption controls the methane adsorption process.

Data Availability

All data generated or analyzed during this study are included in this manuscript.

Conflicts of Interest

The authors state that there is no conflict of interest in this study.

References

[1] IEA, *World Energy Outlook 2018*, IEA, Paris, 2018, https://www.iea.org/reports/world-energy-outlook-2018.

[2] V. Arutyunov, M. Y. Bykhovskii, M. Y. Sinev, and V. Korchak, "Oxidative conversion of hexane as a model of selective conversion of heavy components of hydrocarbon gases," *Russian Chemical Bulletin*, vol. 59, no. 8, pp. 1528–1532, 2010.

[3] S. Alhasan, R. Carriveau, and D.-K. Ting, "A review of adsorbed natural gas storage technologies," *International Journal of Environmental Studies*, vol. 73, no. 3, pp. 343–356, 2016.

[4] T. A. Makal, J.-R. Li, W. Lu, and H.-C. Zhou, "Methane storage in advanced porous materials," *Chemical Society Reviews*, vol. 41, no. 23, pp. 7761–7779, 2012.

[5] J. Wang, L. Huang, R. Yang et al., "Recent advances in solid sorbents for CO2capture and new development trends," *Energy & Environmental Science*, vol. 7, no. 11, pp. 3478–3518, 2014.

[6] T. Kopac, "Hydrogen storage characteristics of bio-based porous carbons of different origin: a comparative review," *International Journal of Energy Research*, vol. 45, no. 15, pp. 20497–20523, 2021.

[7] R. B. Rios, F. W. M. Silva, A. E. B. Torres, D. C. Azevedo, and C. L. Cavalcante, "Adsorption of methane in activated carbons obtained from coconut shells using H3PO4 chemical activation," *Adsorption*, vol. 15, no. 3, pp. 271–277, 2009.

[8] A. Toprak and T. Kopac, "Effect of surface area and micropore volume of activated carbons from coal by Koh, naoh and zncl2 treatments on methane adsorption," *International Journal of Chemical Reactor Engineering*, vol. 17, 2019.

[9] M. S. Balathanigaimani, H.-C. Kang, W.-G. Shim, C. Kim, J.-W. Lee, and H. Moon, "Preparation of powdered activated carbon from rice husk and its methane adsorption properties," *Korean Journal of Chemical Engineering*, vol. 23, no. 4, pp. 663–668, 2006.

[10] E. Salehi, V. Taghikhani, C. Ghotbi, E. N. Lay, and A. Shojaei, "Theoretical and experimental study on the adsorption and desorption of methane by granular activated carbon at 25°C," *Journal of Natural Gas Chemistry*, vol. 16, no. 4, pp. 415–422, 2007.

[11] S. L. James, "Metal-organic frameworks," *Chemical Society Reviews*, vol. 32, no. 5, pp. 276–288, 2003.

[12] X.-W. Liu, T.-J. Sun, J.-L. Hu, and S.-D. Wang, "Composites of metal–organic frameworks and carbon-based materials: preparations, functionalities and applications," *Journal of Materials Chemistry A*, vol. 4, no. 10, pp. 3584–3616, 2016.

[13] M. Kondo, T. Yoshitomi, H. Matsuzaka, S. Kitagawa, and K. Seki, "Three-dimensional framework with channeling cavities for small molecules: $\{[M_2(4,\ 4'\text{-bpy})_3(NO_3)_4]\cdot xH_2O\}_n$ (M = Co, Ni, Zn)," *Angewandte Chemie International Edition*, vol. 36, no. 16, pp. 1725–1727, 1997.

[14] W. Zhou, "Methane storage in porous metal–organic frameworks: current records and future perspectives," *The Chemical Record*, vol. 10, no. 3, pp. 200–204, 2010.

[15] M. Eddaoudi, J. Kim, N. Rosi et al., "Systematic design of pore size and functionality in isoreticular mofs and their application in methane storage," *Science*, vol. 295, no. 5554, pp. 469–472, 2002.

[16] I. Senkovska and S. Kaskel, "High pressure methane adsorption in the metal-organic frameworks $Cu_3(btc)_2$, $Zn_2(bdc)_2$dabco, and $Cr_3F(H_2O)_2O(bdc)_3$," *Microporous and Mesoporous Materials*, vol. 112, no. 1-3, pp. 108–115, 2008.

[17] Y. He, W. Zhou, G. Qian, and B. Chen, "Methane storage in metal–organic frameworks," *Chemical Society Reviews*, vol. 43, no. 16, pp. 5657–5678, 2014.

[18] K. Seki, S. Takamizawa, and W. Mori, "Characterization of microporous copper(II) dicarboxylates (fumarate, terephthalate, andtrans-1,4-cyclohexanedicarboxylate) by gas adsorption," *Chemistry Letters*, vol. 30, no. 2, pp. 122-123, 2001.

[19] D. Bradshaw, A. Garai, and J. Huo, "Metal–organic framework growth at functional interfaces: thin films and composites for diverse applications," *Chemical Society Reviews*, vol. 41, no. 6, pp. 2344–2381, 2012.

[20] A. Corma, H. I. Garcia, and F. X. Llabrés i Xamena, "Engineering metal organic frameworks for heterogeneous catalysis," *Chemical Reviews*, vol. 110, no. 8, pp. 4606–4655, 2010.

[21] J. Lee, O. K. Farha, J. Roberts, K. A. Scheidt, S. T. Nguyen, and J. T. Hupp, "Metal–organic framework materials as catalysts," *Chemical Society Reviews*, vol. 38, no. 5, pp. 1450–1459, 2009.

[22] C. Petit and T. J. Bandosz, "Engineering the surface of a new class of adsorbents: metal-organic framework/graphite oxide composites," *Journal of Colloid and Interface Science*, vol. 447, pp. 139–151, 2015.

[23] Z. Zhang, H. Wang, X. Chen, C. Zhu, W. Wei, and Y. Sun, "Chromium-based metal–organic framework/mesoporous carbon composite: synthesis, characterization and co 2 adsorption," *Adsorption*, vol. 21, no. 1-2, pp. 77–86, 2015.

[24] S. Li and F. Huo, "Metal–organic framework composites: from fundamentals to applications," *Nanoscale*, vol. 7, no. 17, pp. 7482–7501, 2015.

[25] Q.-L. Zhu and Q. Xu, "Metal–organic framework composites," *Chemical Society Reviews*, vol. 43, no. 16, pp. 5468–5512, 2014.

[26] E. Frackowiak and F. Beguin, "Carbon materials for the electrochemical storage of energy in capacitors," *Carbon*, vol. 39, no. 6, pp. 937–950, 2001.

[27] Z. Xu and C. Gao, "Graphene fiber: a new trend in carbon fibers," *Materials Today*, vol. 18, no. 9, pp. 480–492, 2015.

[28] I. Ahmed and S. H. Jhung, "Composites of metal-organic frameworks: preparation and application in adsorption," *Materials Today*, vol. 17, no. 3, pp. 136–146, 2014.

[29] N. M. Mahmoodi, M. Oveisi, M. Bakhtiari et al., "Environmentally friendly ultrasound-assisted synthesis of magnetic zeolitic imidazolate framework - graphene oxide nanocomposites and pollutant removal from water," *Journal of Molecular Liquids*, vol. 282, pp. 115–130, 2019.

[30] S. S. Kaye, A. Dailly, O. M. Yaghi, and J. R. Long, "Impact of preparation and handling on the hydrogen storage properties of zn4o (1, 4-benzenedicarboxylate) 3 (mof-5)," *Journal of the American Chemical Society*, vol. 129, no. 46, pp. 14176-14177, 2007.

[31] A. H. Khoshakhlagh, F. Golbabaei, M. Beygzadeh, F. Carrasco-Marín, and S. J. Shahtaheri, "Toluene adsorption on porous cu–bdc@ oac composite at various operating conditions: optimization by response surface methodology," *RSC Advances*, vol. 10, no. 58, pp. 35582–35596, 2020.

[32] B. Chen, X. Wang, Q. Zhang et al., "Synthesis and characterization of the interpenetrated mof-5," *Journal of Materials Chemistry*, vol. 20, no. 18, pp. 3758–3767, 2010.

[33] C. G. Carson, K. Hardcastle, J. Schwartz et al., "Synthesis and structure characterization of copper terephthalate metal–organic frameworks," vol. 2009, Tech. Rep. 16, Wiley Online Library, 2009.

[34] K. Huang, Y. Xu, L. Wang, and D. Wu, "Heterogeneous catalytic wet peroxide oxidation of simulated phenol wastewater by copper metal–organic frameworks," *RSC Advances*, vol. 5, no. 41, pp. 32795–32803, 2015.

[35] N. E. Tari, A. Tadjarodi, J. Tamnanloo, and S. Fatemi, "Facile and fast, one pot microwave synthesis of metal organic framework copper terephthalate and study co2 and ch4 adsorption on it," *Journal of Porous Materials*, vol. 22, no. 5, pp. 1161–1169, 2015.

[36] H. Kakaei, M. Beygzadeh, F. Golbabaei, M. R. Ganjali, M. Jahangiri, and S. J. Shahtaheri, "Preparation of a sepiolite/cu-bdc nanocomposite and its application as an adsorbent in respirator cartridges for H2S removal," *New Journal of Chemistry*, vol. 43, no. 29, pp. 11575–11584, 2019.

[37] H. Kim, D. G. Samsonenko, S. Das et al., "Methane sorption and structural characterization of the sorption sites in Zn2(bdc)2(dabco) by single crystal X-ray crystallography," *Chemistry–An Asian Journal*, vol. 4, no. 6, pp. 886–891, 2009.

[38] D. Z. Li, L. Chen, G. Liu et al., "Porous metal-organic frameworks for methane storage and capture: status and challenges," *New Carbon Materials*, vol. 36, no. 3, pp. 468–496, 2021.

[39] E. Tsivion and M. Head-Gordon, "Methane storage: molecular mechanisms underlying room-temperature adsorption in zn4o (bdc) 3 (mof-5)," *The Journal of Physical Chemistry C*, vol. 121, no. 22, pp. 12091–12100, 2017.

[40] H. Li, L. Li, R.-B. Lin et al., "Porous metal-organic frameworks for gas storage and separation: status and challenges," *EnergyChem*, vol. 1, no. 1, article 100006, 2019.

[41] Y. He, F. Chen, B. Li, G. Qian, W. Zhou, and B. Chen, "Porous metal-organic frameworks for fuel storage," *Coordination Chemistry Reviews*, vol. 373, pp. 167–198, 2018.

[42] T. Düren, L. Sarkisov, O. M. Yaghi, and R. Q. Snurr, "Design of new materials for methane storage," *Langmuir*, vol. 20, no. 7, pp. 2683–2689, 2004.

[43] H. Wu, W. Zhou, and T. Yildirim, "High-capacity methane storage in metal– organic frameworks m2 (dhtp): the important role of open metal sites," *Journal of the American Chemical Society*, vol. 131, no. 13, pp. 4995–5000, 2009.

[44] H. Zhou, S. Zhu, I. Honma, and K. Seki, "Methane gas storage in self-ordered mesoporous carbon (cmk-3)," *Chemical Physics Letters*, vol. 396, no. 4-6, pp. 252–255, 2004.

[45] N. E. Tari, A. Tadjarodi, J. Tamnanloo, and S. Fatemi, "Synthesis and property modification of MCM-41 composited with Cu(BDC) MOF for improvement of CO_2 adsorption Selectivity," *Journal of CO2 Utilization*, vol. 14, pp. 126–134, 2016.

[46] M. Khalili, E. Ganji, A. Taheri, and M. Pourkhalil, "Adsorption of ch4 and co2 on cu-bdc metal-organic frameworks synthesized using different solvent separation routes," *Journal of Petroleum Science and Technology*, vol. 10, pp. 12–19, 2020.

[47] M. Anbia and S. Sheykhi, "Preparation of multi-walled carbon nanotube incorporated MIL-53-Cu composite metal-organic framework with enhanced methane sorption," *Journal of Industrial and Engineering Chemistry*, vol. 19, no. 5, pp. 1583–1586, 2013.

[48] M. Arnold, P. Kortunov, D. J. Jones, Y. Nedellec, J. Kärger, and J. Caro, *Oriented crystallisation on supports and anisotropic mass transport of the metal-organic framework manganese formate*, vol. 2007, no. 1, 2007Wiley Online Library, 2007.

[49] N. S. Nasria, H. U. Sidikc, M. A. A. Zainib et al., "Kinetic equilibrium and isotherm modeling adsorbed methane assessment on synthesized peek-porous sorbent carbon of sustainable coconut shell kernel," *Chemical Engineering*, vol. 72, 2019.

[50] A. Almasian, N. M. Mahmoodi, and M. E. Olya, "Tectomer grafted nanofiber: synthesis, characterization and dye removal ability from multicomponent system," *Journal of Industrial and Engineering Chemistry*, vol. 32, pp. 85–98, 2015.

[51] N. M. Mahmoodi, M. Ghezelbash, M. Shabanian, F. Aryanasab, and M. R. Saeb, "Efficient removal of cationic dyes from colored wastewaters by dithiocarbamate-functionalized graphene oxide nanosheets: from synthesis to detailed kinetics studies," *Journal of the Taiwan Institute of Chemical Engineers*, vol. 81, pp. 239–246, 2017.

[52] F. O. Erdogan and T. Kopac, "Highly effective activated carbons from Turkish–Kozlu bituminous coal by physical and Koh activation and sorption studies with organic vapors," *International Journal of Chemical Reactor Engineering*, vol. 17, 2019.

[53] K. Y. Foo and B. H. Hameed, "Insights into the modeling of adsorption isotherm systems," *Chemical Engineering Journal*, vol. 156, no. 1, pp. 2–10, 2010.

[54] I. Langmuir, "The adsorption of gases on plane surfaces of glass, mica and platinum," *Journal of the American Chemical Society*, vol. 40, no. 9, pp. 1361–1403, 1918.

[55] D. Langmuir and J. S. Herman, "The mobility of thorium in natural waters at low temperatures," *Geochimica et Cosmochimica Acta*, vol. 44, no. 11, pp. 1753–1766, 1980.

[56] J. A. Mason, M. Veenstra, and J. R. Long, "Evaluating metal–organic frameworks for natural gas storage," *Chemical Science*, vol. 5, no. 1, pp. 32–51, 2014.

[57] A. Adamsom and A. Gast, "Physical chemistry of surfaces," *A Wiley-Interscience Publication*, 1997.